Catalytic performance and characterization of RhVO$_4$/SiO$_2$ for hydroformylation and CO hydrogenation

Takashi Yamagishi [a], Ippei Furikado [a], Shin-ichi Ito [a], Toshihiro Miyao [b],
Shuichi Naito [b], Keiichi Tomishige [a,**], Kimio Kunimori [a,*]

[a] *Institute of Materials Science, University of Tsukuba, 1-1-1, Tennodai, Tsukuba, Ibaraki 305-8573, Japan*
[b] *Department of Applied Chemistry, Faculty of Engineering, Kanagawa University, 3-27-1, Rokkakubashi, Kanazawa-ku, Yokohama 221-8686, Japan*

Abstract

Effect of addition of vanadium oxide (vanadia) to Rh/SiO$_2$ in hydroformylation of ethylene and CO hydrogenation was investigated. In the hydroformylation of ethylene, the addition of vanadia enhanced hydroformylation activity and selectivity; especially the selectivity for 1-propanol formation was drastically promoted. The promoting effect was observed more significantly on the catalyst calcined at higher temperature such as 973 K. It is found that the effect is related to the formation of the RhVO$_4$ phase, and it is suggested that the active site consists of Rh metal and partially reduced VO$_x$, which is formed by the reduction of RhVO$_4$. This can make the interaction between Rh and VO$_x$ more intimate. This catalyst was also effective for the alcohol formation in CO hydrogenation. Based on the catalyst characterization by means of the adsorption measurements of H$_2$ and CO, H$_2$–D$_2$ exchange rate under the presence of CO, temperature-programmed desorption (TPD) of CO, temperature-programmed reduction (TPR) with H$_2$ and temperature-programmed surface reaction (TPSR) of adsorbed CO with H$_2$, it is suggested that the sites for H$_2$ activation, which cannot be inhibited by the presence of CO, play an important role in the promotion of alcohol formation in hydroformylation and CO hydrogenation.
© 2005 Elsevier B.V. All rights reserved.

Keywords: Hydroformylation; Ethylene; 1-Propanol; RhVO$_4$; SMOI; Rh–VO$_x$ interaction

1. Introduction

Hydroformylation is one of important industrial processes for producing oxygen-containing compounds (especially aldehyde) from olefin. Therefore, the catalysts for the gas phase [1–3] and liquid phase [4–7] hydroformylation have been developed. It is well known that Rh is active species for hydroformylation reaction. Especially the additive effect of various components over heterogeneous Rh catalysts has been investigated in order to enhance the catalytic activity and selectivity [1,8–15]. In hydroformylation reaction, the insertion of CO to an alkyl group is an important elementary step. In addition, it has been reported that Rh is an effective species for C2 oxygenates formation in CO hydrogenation [3]. This property is related to high performance in CO insertion. There are also reports on addition of metal or metal oxide to Rh-based catalysts for CO hydrogenation [1,8,11,16–27]. In both reactions, the additives produced a significant effect on conversion and product distribution. In many cases, the interaction between Rh and additive component is important in the catalytic promotion mechanism, especially if the additive can be located near Rh site in an atomic scale [20,28–30].

One method for making the intimate interaction is preparation of catalysts via mixed oxide crystallites [22–25,31,32]. Our group has found that mixed oxides such as RhVO$_4$, RhNbO$_4$ and Rh$_2$MnO$_4$ can be formed on SiO$_2$ support by the calcination at high temperature (973–1173 K) [22,24]. RhVO$_4$ was decomposed to highly dispersed Rh metal particles covered with partially reduced vanadia species (VO$_x$) by H$_2$ reduction above 473 K, and a strong metal–oxide (Rh–VO$_x$) interaction (SMOI) was induced on SiO$_2$ support [22,23,25].

In this article, we investigated the performance of vanadia promoted Rh/SiO$_2$ (V–Rh/SiO$_2$) catalysts prepared via RhVO$_4$ mixed oxide in hydroformylation of olefins (ethylene and propylene) and CO hydrogenation under atmospheric pressure. In addition, from the catalyst characterization data, the mechanism of the promotion by vanadium oxide is discussed.

2. Experimental

2.1. Catalyst preparation

All catalysts were prepared by impregnating SiO$_2$ support (Q-100 or G-6; Fuji Silysia Chemical Ltd.) with aqueous solution of metal salts. Before the impregnation, SiO$_2$ was calcined in air at 1173 K for 1 h to avoid the structural change during the catalyst preparation. The BET surface areas of the SiO$_2$ (Q-100 and G-6) after the calcination were 38 and 535 m^2/g, respectively. Rh/SiO$_2$ (Q-100 and G-6) catalysts were prepared by the incipient wetness method using RhCl$_3$·3H$_2$O (N.E. Chemcat Corporation, >98%). Unless otherwise stated, the SiO$_2$ (Q-100) support was used. The method of preparing modified Rh catalysts (M-Rh/SiO$_2$, M = V, Fe, Zn, Mo, Co, Zr and Nb) was as follows: after the impregnation of SiO$_2$ with RhCl$_3$·3H$_2$O aqueous solution and drying at 383 K for 12 h, the modification with additive component was carried out by the subsequent impregnation using the aqueous solution of NH$_4$VO$_3$ (WAKO Pure Chemical Industries Ltd., >99.5%), Fe(NO$_3$)$_3$·9H$_2$O (WAKO Pure Chemical Industries Ltd., >99%), Zn(NO$_3$)$_2$·6H$_2$O (WAKO Pure Chemical Industries Ltd., >99%), (NH$_4$)$_6$Mo$_7$O$_{24}$·4H$_2$O (WAKO Pure Chemical Industries Ltd., >99%), Co(NO$_3$)$_2$·6H$_2$O (WAKO Pure Chemical Industries Ltd., >98%), ZrO(NO$_3$)$_2$·2H$_2$O (SOEKAWA CHEMICALS, >99%) and (NH$_4$)$_3$[NbO(C$_2$O$_4$)$_3$] (CBMM International LDTA, AD-382). After the catalysts were dried at 383 K for 12 h again, they were calcined in air at 573–973 K for 3 h. The loading amount of Rh was 4 wt%, and the amount of additive was adjusted to molar ratio of M/Rh = 1. V$_2$O$_5$/SiO$_2$ was prepared by impregnating SiO$_2$ (Q-100) with the aqueous solution of NH$_4$VO$_3$. After the sample was dried at 383 K for 12 h, it was calcined at 773 K for 3 h. Loading amount of vanadium was adjusted to that of V–Rh/SiO$_2$.

2.2. Catalyst characterization

X-ray diffraction (XRD) measurements were carried out with an X-ray diffractometer (Philips X'Pert MRD) equipped with a graphite monochromator for Cu Kα (40 kV, 20 mA) radiation. The mean particle size was calculated from the XRD line broadening measurement using Scherrer equation [31,33]. Transmission electron microscope (TEM, JEOL JEM-2010) observation was carried out for V–Rh/SiO$_2$ catalysts after reduction, CO hydrogenation and ethylene hydroformylation. The amounts of H$_2$ and CO chemisorption were measured in a conventional volumetric adsorption apparatus; detailed procedures were described elsewhere [34,35]. The amounts of the total H$_2$ chemisorption (H/Rh) and the irreversible CO chemisorption (CO/Rh) were measured at room temperature after H$_2$ reduction and evacuation at 573 K.

Temperature-programmed reduction (TPR) was carried out in a fix bed reactor equipped with a TCD detector using 5% H$_2$ diluted with Ar (30 ml/min). The amount of catalyst was 0.05 g, and the temperature was increased from room temperature to 1123 K at the heating rate of 10 K/min. Temperature-programmed desorption (TPD) of CO adsorbed on the catalyst was carried out in a closed circulation system equipped with a quadrupole mass spectrometer (Balzers QMS 200F). The amount of the catalyst was 0.10 g and the temperature was increased from room temperature to 773 K at the rate of 10 K/min. The catalyst was exposed to CO (7 kPa) at room temperature after reduction in H$_2$ (7 kPa) and evacuation at 573 K before TPD measurements.

Temperature-programmed surface reaction (TPSR) of adsorbed CO with H$_2$ was carried out in the fixed bed flow reactor under atmospheric pressure. The effluent gas was analyzed by FID-gas chromatograph (Shimadzu GC-14B) equipped with a methanator using a Gaschropak 54 column every 30 s. The catalyst weight was 0.1 g, and the temperature was increased from room temperature to 600 K at the heating rate of 10 K/min under the flow of 10% H$_2$ (total flow rate: 10 ml/min, balanced with He). The catalyst was exposed to CO (5 kPa, total flow rate 10 ml/min, balanced with He) at room temperature after H$_2$ reduction and purge with He at 573 K before TPSR measurements.

Fourier transform infrared spectra (FTIR) of CO adsorption was recorded at room temperature by an FTIR spectrometer (Nicolet, Magna-IR 550 spectrometer) in the transmission mode using a quartz glass IR cell with CaF$_2$ windows connected to the vacuum-closed circulating system. The catalyst was well mixed with the same weight of SiO$_2$ (fine powder, AEROSIL SiO$_2$ 380, BET 380 m^2/g), and it was pressed into a disk of 20 mm Ø and a weight of about 0.03 g. The catalyst was exposed to CO (7 kPa) at room temperature after the reduction with 7 kPa H$_2$ and evacuation at 573 K. After CO adsorption, the gas was evacuated. FTIR spectra of adsorbed CO were obtained under vacuum. H$_2$–D$_2$ exchange reaction under presence of CO was carried out in the closed circulation system equipped with the quadrupole mass spectrometer. The catalyst amount was 0.5 g, and the catalyst sample was reduced in 33.3 kPa of H$_2$ at 573 K for Rh-based catalyst and at 1023 K for V$_2$O$_5$/SiO$_2$, and subsequently evacuated at the same temperature. After the temperature reached the reaction temperature, reactant gases ($P_{H_2} = P_{D_2} = P_{CO} = 20$ kPa, $P_{Ar} = 6$ kPa as internal standard gas) were introduced and they were continuously circulated during the reaction. The reaction was carried out in the range of room temperature to 353 K, and the gas phase was analyzed by the quadrupole mass spectrometer every 4.5 min.

2.3. Hydroformylation of ethylene and propylene

Ethylene hydroformylation was carried out in the fixed bed flow reactor system under atmospheric pressure. The catalyst was pretreated under hydrogen flow (30 ml/min) at 573 K for 1 h. After the reactor was cooled down to room temperature, the reactant gases for hydroformylation of ethylene ($P_{C_2H_4} = P_{CO} = P_{H_2} = 33.8$ kPa) were fed to the catalyst bed, and then

the reaction temperature increased step-by-step and it was kept for about 1.5 h at each reaction temperature. The effluent gas was analyzed by a gas chromatograph (GC). Ethylene and ethane were analyzed by an FID-GC (Shimadzu GC-14B) using VZ-10 column (3 mm i.d., 2 m). Oxygenates were analyzed by FID-GC (Shimadzu GC-8A) using a Stabilwax fused silica capillary column (RESTEK, 0.53 mm i.d., 60 m). Carbon monoxide was analyzed by a TCD-GC (Shimadzu GC-8A) using a Porapak Q column (3 mm i.d., 2 m). The catalyst amount was 0.1 g, and the total flow rate of the reactant gases was 6 ml/min, which corresponded to GHSV = 3600 h^{-1}. Hydroformylation of propylene was also carried out in a similar method to that of ethylene.

2.4. CO hydrogenation

CO hydrogenation reaction was carried out in the fixed bed flow reactor at atmospheric pressure. After 0.5 g of catalyst was reduced in H$_2$ flow (30 ml/min) at 573 K, the reactant gas ($P_{CO} = 33.8$ kPa, $P_{H_2} = 67.6$ kPa, total flow rate 1.5 ml/min, GHSV = 180 h^{-1}) was fed into the reactor at room temperature, and then the reaction temperature increased step-by-step. Although the catalyst activity changed with time on stream, especially at the initial stage, steady-state activity could be obtained after about 1.5 h. The steady-state activity was compared. CO and CO$_2$ were analyzed with TCD-GC (Shimadzu GC-8A) equipped with a Porapak Q column (3 mm i.d., 2 m), and product hydrocarbons and oxygenates were analyzed with an FID-GC (Shimadzu GC-8A) using a Rt-UPLOT fused silica capillary column (RESTEK, 0.32 mm i.d., 30 m).

2.5. Hydrogenation of propanal under presence of CO

In order to elucidate the formation mechanism of alcohol in hydroformylation and CO hydrogenation, hydrogenation of propanal under the presence of CO was carried out in the fixed bed flow reactor under atmospheric pressure. After the catalysts were pretreated in flowing hydrogen (30 ml/min) at 573 K, the reactant gas ($P_{propanal} = 0.17$ kPa, $P_{CO} = P_{H_2} = 33.8$ kPa, balanced with He) was fed into the reactor in the temperature range of 373–433 K. The effluent gas was analyzed in a way similar to that in the hydroformylation of ethylene.

3. Results and discussion

3.1. Effect of vanadia in hydroformylation

Fig. 1 shows reaction time dependence of ethylene hydroformylation activity over V–Rh/SiO$_2$ catalyst calcined at 973 K followed by H$_2$ reduction at 573 K. During the first 1 h, the conversion and selectivity was changed significantly; however, there was not much change in the activity after 1 h. Therefore, the activity at 1.5 h is compared hereafter. Ethylene-based conversion increased gradually with time on stream. Selectivity changed more significantly than conversion. The selectivity for ethane formation gradually decreased, but in contrast, that of 1-propanol formation increased with time on stream. Takahashi et al. have reported that propanal yield increased at the initial
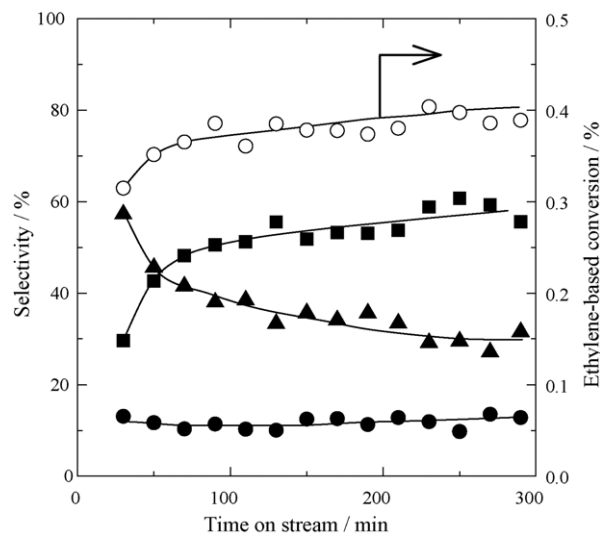

Fig. 1. Reaction time dependence of ethylene hydroformylation selectivity and ethylene-based conversion over V–Rh/SiO$_2$ at 388 K: (■) 1-propanol, (●) propanal, (▲) ethane and (○) ethylene-based conversion. Reaction conditions: catalyst weight = 0.1 g, $P_{C_2H_4} = P_{CO} = P_{H_2} = 33.8$ kPa, total flow rate = 6 ml/min, total pressure = 0.1 MPa and reduction temperature = 573 K.

stage of hydroformylation reaction and that was due to adsorption of propanal and higher compounds formation on catalyst support [36]. However, this is not consistent with the behavior of propanal since the formation rate of propanal was stable from the initial stage. Therefore, we assume that the active site for ethylene hydrogenation was changed to that for 1-propanol formation, although details are not clear at present.

Reaction temperature dependence of ethylene hydroformylation over V–Rh/SiO$_2$ calcined at 973 K followed by H$_2$ reduction at 573 K is shown in Fig. 2. Ethylene conversion increased
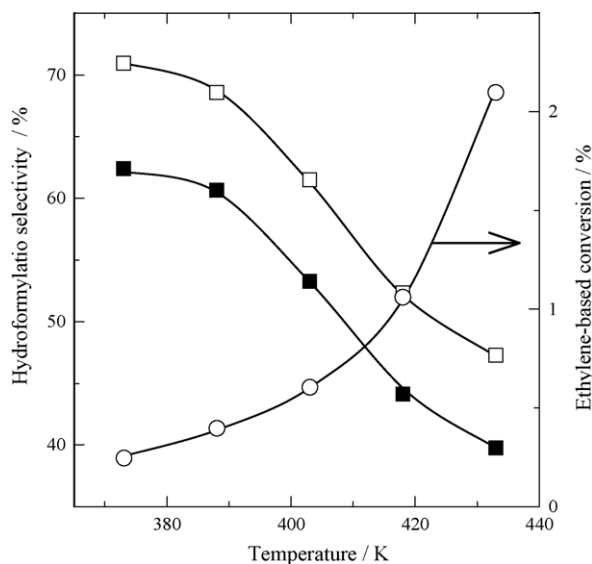

Fig. 2. Reaction temperature dependence of ethylene hydroformylation over V–Rh/SiO$_2$ catalyst calcined at 973 K: (○) ethylene-based conversion, (□) selectivity to oxygenates (oxygenates = 1-propanol + propanal) and (■) selectivity to 1-propanol. Reaction conditions: catalyst weight = 0.1 g, $P_{C_2H_4} = P_{CO} = P_{H_2} = 33.8$ kPa, total flow rate = 6 ml/min, total pressure = 0.1 MPa and reduction temperature = 573 K.

Table 1
Activation energy of ethylene hydroformylation over Rh/SiO$_2$ and V–Rh/SiO$_2$ catalysts

Catalyst	Support	Activation energy (kJ/mol)			Reference
		1-Propanol	Propanal	Ethane	
Rh/SiO$_2$[a]	Q-100	–	60	65	This work
Rh/SiO$_2$[b]	G-6	–	44	78	This work
V–Rh/SiO$_2$[b]	Q-100	37	47	62	This work
Rh/SiO$_2$	–	–	–	57	88	[37]
	–	–	–	50	87	[38]

[a] Temperature range was 413–483 K.
[b] Temperature range was 373–433 K.

with increasing reaction temperature; however, the selectivity to oxygenate compounds (1-propanol + propanal) decreased. This temperature dependence is usually observed in hydroformylation of ethylene. In this temperature range, the main product of oxygenates was 1-propanol over the V–Rh/SiO$_2$ catalyst. The activation energy of ethylene hydroformylation over Rh/SiO$_2$ and V–Rh/SiO$_2$ is listed in Table 1. In the case of Rh/SiO$_2$, the activation energy of propanal formation was lower than that of ethane formation. This tendency is consistent with that reported [37,38]. The activation energy of 1-propanol formation over the V–Rh/SiO$_2$ catalyst calcined at 973 K was estimated to be 37 kJ/mol, which was lower than the others, and this can be related to the high selectivity for 1-propanol formation.

Activity of various Rh-based catalysts for ethylene hydroformylation is listed in Table 2. We prepared two kinds of Rh/SiO$_2$ using different SiO$_2$ supports. The amounts of H$_2$ and CO adsorption are listed in Table 3. The results show that Rh metal particles were much more dispersed over Rh/SiO$_2$ (G-6) than over Rh/SiO$_2$ (Q-100), being highly dependent on the surface area of the support. As listed in Table 2, Rh/SiO$_2$ (G-6) exhibited much higher conversion than Rh/SiO$_2$ (Q-100), which

can be explained by the metal dispersion. Furthermore, the selectivity for hydroformylation over Rh/SiO$_2$ (G-6) was also higher than that over Rh/SiO$_2$ (Q-100). It has been reported that the selectivity for hydroformylation is higher over more highly dispersed Rh metal particles [39,40]. In addition, it is very important to note that the selectivity for 1-propanol is almost zero over both Rh/SiO$_2$ catalysts. We prepared V–Rh/SiO$_2$ using SiO$_2$ (Q-100) because RhVO$_4$ was formed by the stoichiometric surface reaction between Rh and V. When SiO$_2$ (G-6) was used, the interaction was weak, and the effect of V addition was not remarkable. This is why we used SiO$_2$ (Q-100). Over the V–Rh/SiO$_2$ catalysts 1-propanol was mainly formed. The performance was dependent on the calcination temperature, and the catalyst calcined at 973 K was more effective than that calcined at 773 K. The performance of V–Rh/SiO$_2$ was compared to that of M-Rh/SiO$_2$ catalysts as listed in Table 2. According to the previous reports, 1-propanol was obtained efficiently in hydroformylation of ethylene over Rh catalysts modified with Fe, Zn and Mo [1,8,11]. Therefore, we prepared and tested them. As shown in Table 2, the addition of various components promoted 1-propanol formation in ethylene hydroformylation. In the case of Mo-Rh/SiO$_2$, the selectivity for 1-propanol and the hydroformylation product (1-propanol + propanal) was high; however, the selectivity for ethane formation was much higher than that over Rh/SiO$_2$, although the conversion was significantly high. Other additives did not lead to any attractive selectivity. Thus, vanadia is the most effective additive. In addition, the effect of calcination temperature over M-Rh/SiO$_2$ (M = Mo, Zn and Fe) on the catalyst performance is different from that over V–Rh/SiO$_2$. In the case of M-Rh/SiO$_2$ (M = Mo, Zn and Fe), increasing calcination temperature decreased the conversion and hydroformylation selectivity.

Furthermore, we also tested hydroformylation of propylene as listed in Table 4. Over V–Rh/SiO$_2$ the propylene conversion increased with increasing calcination temperature, and the

Table 2
Results of ethylene hydroformylation over Rh-based catalyst on SiO$_2$ at 388 K

Catalyst	Support	Calcination temperature (K)	Conversion (%)	Yield (10^{-2}%)			Selectivity (%)		
				1-Propanol	Propanal	Ethane	1-Propanol	Propanal	Ethane
Rh/SiO$_2$	Q-100	773	0.21	0	8	13	0	38	62
	G-6	773	1.88	1	123	64	<1	65	34
V–Rh/SiO$_2$	Q-100	773	0.20	12	1	7	57	7	36
	Q-100	973	0.40	24	3	13	61	8	31
Mo-Rh/SiO$_2$	Q-100	773	1.30	53	5	72	41	4	55
	Q-100	973	0.71	22	1	48	31	1	68
Zn-Rh/SiO$_2$	Q-100	773	0.22	7	11	4	32	50	18
	Q-100	973	0.07	2	2	3	22	33	45
Fe-Rh/SiO$_2$	Q-100	773	0.48	10	17	21	21	35	44
	Q-100	973	0.08	1	2	5	17	23	60
Co-Rh/SiO$_2$	Q-100	773	0.69	6	34	29	9	49	42
Zr-Rh/SiO$_2$	Q-100	773	1.16	32	42	42	28	36	36
Nb-Rh/SiO$_2$	Q-100	773	0.39	4	14	21	10	36	54

Yield and selectivity were calculated on the ethylene basis. Reaction conditions: catalyst weight = 0.1 g, $P_{C_2H_4} = P_{CO} = P_{H_2} = 33.8$ kPa, total flow rate = 6 ml/min, total pressure = 0.1 MPa and reduction temperature = 573 K.

Table 3
Characterization of Rh/SiO$_2$ and V–Rh/SiO$_2$ by means of adsorption and XRD

Catalyst	Support	Calcination temperature (K)	XRD		Adsorption		TOF[c] (10^{-2} min^{-1})		
			Particle size[a] (nm)	Dispersion of Rh metal[b]	H/Rh	CO/Rh	1-Propanol	Propanal	Ethane
Rh/SiO$_2$	Q-100	773	14	0.08	0.04	0.04	0.0	4.8	7.1
	G-6	773	2.9	0.38	0.50	0.45	<0.1	5.5	3.4
V–Rh/SiO$_2$	Q-100	773	2.6	0.42	0.28	0.08	3.6	0.4	2.2
	Q-100	973	3.0	0.37	0.17	0.06	10.1	1.3	5.2

All samples were reduced at 573 K before the characterization.
[a] Calculated from XRD line broadening measurement using Scherrer equation [31,33].
[b] Dispersion of Rh metal is calculated on the basis of 1.1/d (particle size, nm) [34].
[c] Calculated from CO uptake and formation rate of each product in ethylene hydroformylation at 388 K.

hydroformylation selectivity was higher than over both Rh/SiO$_2$ catalysts. The TOF of butanol + butanal over V–Rh/SiO$_2$ was also higher than that over Rh/SiO$_2$ catalysts. The most important point is that the selectivity for alcohol formation over V–Rh/SiO$_2$ was much higher than that over Rh/SiO$_2$. The catalytic behavior in propylene hydroformylation was similar to that in ethylene hydroformylation. The n/i ratio was not so different over Rh/SiO$_2$ and V–Rh/SiO$_2$.

3.2. Catalyst characterization

Fig. 3 shows XRD patterns of Rh/SiO$_2$ and M-Rh/SiO$_2$ (M = V, Fe, Zn and Mo) under various treatment conditions. In the case of Rh/SiO$_2$ calcined at 773 K, no peak other than amorphous SiO$_2$ ($2\theta \approx 22°$) was observed (Fig. 3(a)). After the reduction of Rh/SiO$_2$ at 573 K, the peaks assigned to Rh metal were observed (Fig. 3(b)). On the basis of line broadening of the peaks, the mean Rh particle size and the dispersion of Rh metal were estimated as listed in Table 3. In the case of V–Rh/SiO$_2$, no XRD peak assigned to Rh or V species was observed after the calcination at low temperatures such as 573 and 773 K (Fig. 3(c and d)). In contrast, for V–Rh/SiO$_2$ calcined at 873 K, small peaks assigned to RhVO$_4$ [23,25,31] were observed (Fig. 3(e)), and the peak intensity was strong for V–Rh/SiO$_2$ calcined at 973 K (Fig. 3(f)). This indicates that the crystal size of RhVO$_4$ increased with increasing calcination temperature. Furthermore,

after the reduction of V–Rh/SiO$_2$ calcined at 973 K, the broad peak assigned to Rh metal was observed (Fig. 3(g)). This indicates that Rh metal formed on the reduced V–Rh/SiO$_2$ is more highly dispersed than that on Rh/SiO$_2$ even when the low surface area SiO$_2$ was used (Table 3). On the basis of the results that the V–Rh/SiO$_2$ calcined at higher temperature gave higher conversion and selectivity in ethylene hydroformylation, it is thought that the active sites for hydroformylation are formed by the reduction of RhVO$_4$ crystallites. On the other hand, in the XRD patterns of M-Rh/SiO$_2$ (M = Mo, Zn and Fe) calcined at 973 K, the peaks were clearly observed. In the case of Zn-Rh/SiO$_2$ and Mo-Rh/SiO$_2$, the formation of ZnRh$_2$O$_6$ [41] and MoRh$_2$O$_6$ [42,43] was confirmed (Fig. 3(i and j)), respectively. Furthermore, in the case of Fe-Rh/SiO$_2$ catalyst, the peaks were observed between the peaks assigned to Rh$_2$O$_3$ [44] and Fe$_2$O$_3$ [45] (Fig. 3(h)). Since the crystal structure of Rh$_2$O$_3$ and Fe$_2$O$_3$ was similar (rhombohedral), it is suggested that the solid solution of Rh$_2$O$_3$–Fe$_2$O$_3$ can be formed. The results of XRD suggest that mixed oxides were also formed over the M-Rh/SiO$_2$ (M = Mo, Zn and Fe) like V–Rh/SiO$_2$ when the catalysts were calcined at 973 K. In the case of V–Rh/SiO$_2$, it is suggested that the formation of mixed oxide RhVO$_4$ followed by H$_2$ reduction can promote the 1-propanol formation in hydroformylation. The results of two Rh/SiO$_2$ catalysts with different dispersion pointed out that high dispersion of Rh metal is not related to the formation of 1-propanol, although Rh metal particles from

Table 4
Results of propylene hydroformylation over Rh/SiO$_2$ and V–Rh/SiO$_2$

Catalyst	Support	Calcination temperature (K)	Reaction temperature (K)	Conversion (%)	Propylene-based selectivity (%)			TOF[a] (10^{-2} min^{-1})		
					Butanol (n/i)	Butanal (n/i)	Propane	Butanol	Butanal	Propane
Rh/SiO$_2$	Q-100	773	418	0.01	0 (–)	37 (–)	63	0	0.5	0.8
			433	0.05	7 (–)	40 (6.5)	53	0.2	1.1	1.6
	G-6	773	418	0.57	1 (3.5)	33 (2.5)	66	0.0	1.0	1.9
			433	1.26	19 (5.6)	18 (2.8)	63	1.2	1.2	4.0
V–Rh/SiO$_2$	Q-100	773	418	0.11	68 (3.4)	2 (0)	30	2.2	0.1	1.0
			433	0.20	59 (4.8)	2 (0.6)	39	3.4	0.1	2.2
	Q-100	973	418	0.18	51 (3.8)	4 (0.9)	45	3.4	0.2	3.0
			433	0.39	55 (5.2)	3 (1.5)	42	8.3	0.4	6.4

Yield and selectivity were calculated on the propylene basis. Reaction conditions: catalyst weight = 0.1 g, $P_{C_3H_6} = P_{CO} = P_{H_2} = 33.8$ kPa, total flow rate = 6 ml/min, total pressure = 0.1 MPa and reduction temperature = 573 K.
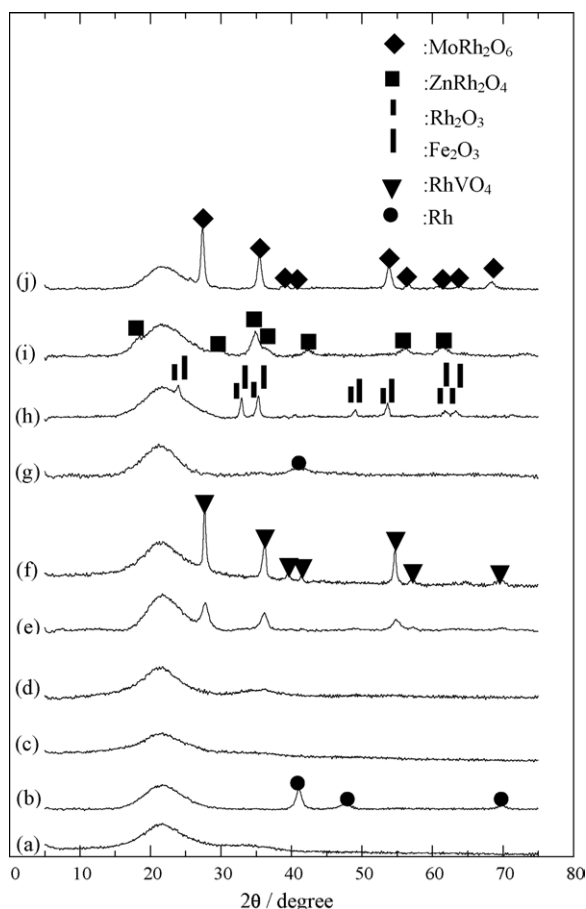[a] Calculated from CO uptake and formation rate of each product in propylene hydroformylation.

Fig. 3. X-ray diffraction patterns of Rh-based catalysts on SiO_2: (a) Rh/SiO_2 calcined at 773 K, (b) sample (a) reduced at 573 K, (c) $V–Rh/SiO_2$ calcined at 573 K, (d) $V–Rh/SiO_2$ calcined at 773 K, (e) $V–Rh/SiO_2$ calcined at 873 K, (f) $V–Rh/SiO_2$ calcined at 973 K, (g) sample (f) reduced at 573 K, (h) $Fe-Rh/SiO_2$ calcined at 973 K, (i) $Zn-Rh/SiO_2$ calcined at 973 K and (j) $Mo-Rh/SiO_2$ calcined at 973 K.

$RhVO_4$ have high dispersion. The mixed oxide derived catalysts were not effective over the $M-Rh/SiO_2$ ($M = Mo$, Zn and Fe).

In order to estimate the interaction between Rh and V oxide on $V–Rh/SiO_2$, the effect of calcination temperature on TPR profiles was investigated (Fig. 4). The consumption amounts of H_2 are listed in Table 5. In the TPR profile of Rh/SiO_2, the reduction proceeded at about 343 K, and this can be assigned to the reduction of Rh_2O_3 to Rh metal, which is supported by the amount of H_2 consumption ($H_2/Rh = 1.5$). On the $V–Rh/SiO_2$
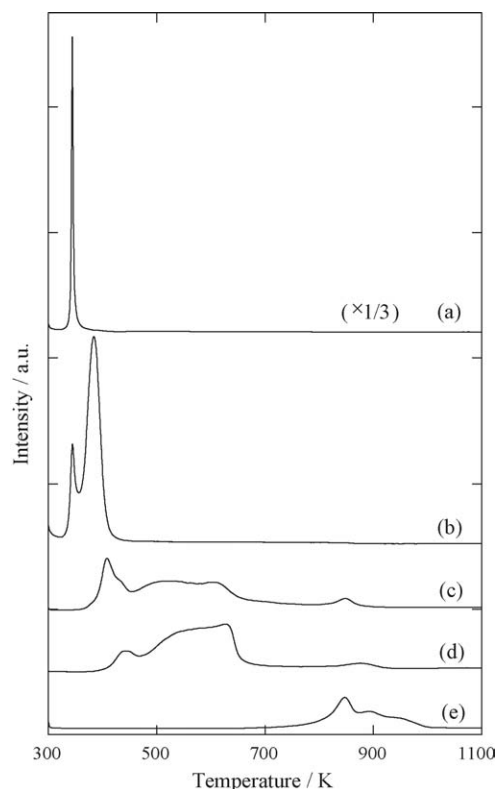

Fig. 4. Temperature-programmed reduction (TPR) profiles of Rh/SiO_2, $V–Rh/SiO_2$ and V_2O_5/SiO_2: (a) Rh/SiO_2 calcined at 773 K, (b) $V–Rh/SiO_2$ calcined at 573 K, (c) 773 K, (d) 973 K and (e) V_2O_5/SiO_2 calcined at 773 K.

calcined at 773 K, the intensity of the peak for Rh_2O_3 reduction decreased and the reduction peak at higher temperature (about 385 K) appeared. The interaction of Rh with V species can decrease reducibility of Rh. On the catalyst calcined at the higher temperature, higher temperature was necessary for the catalyst reduction. It is estimated from the H_2 consumption that Rh is reduced to metal and V_2O_5 is reduced to V_2O_3 (i.e., VO_x, $x = 1.5$). In addition, much higher temperature (850 K) was necessary for the reduction of V_2O_5/SiO_2.

For the characterization of the reduced catalysts, we measured FTIR spectra of CO adsorbed on Rh/SiO_2 and $V–Rh/SiO_2$ catalysts as shown in Fig. 5. On Rh/SiO_2, twin CO (2094 and 2026 cm^{-1}), linear CO (2053 cm^{-1}) and bridge CO (1872 cm^{-1}) were observed [46], and main adsorbed species was the bridge CO. In contrast, on $V–Rh/SiO_2$, twin CO (2094 and 2021 cm^{-1}), linear CO (2053 cm^{-1}) and bridge CO (1913 cm^{-1}) were also

Table 5
H_2 consumption over Rh/SiO_2, $V–Rh/SiO_2$ and V_2O_5/SiO_2 in TPR

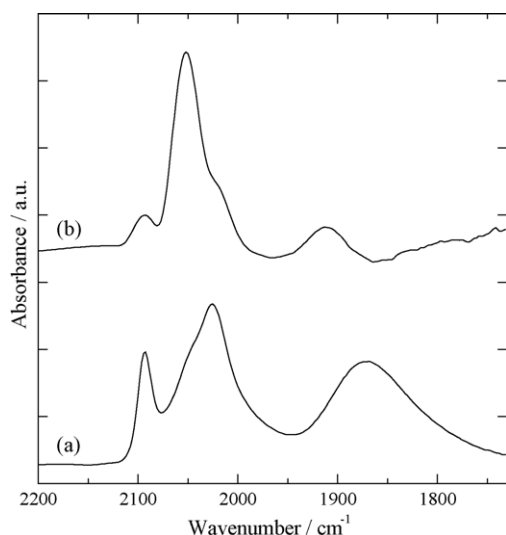| Catalyst	Calcination temperature (K)	Metal content (10^{-4} mol/g cat.)		H_2 consumption (10^{-4} mol/g cat.)[a]
		Rh	V	
Rh/SiO_2	773	3.88	–	5.93
$V–Rh/SiO_2$	773	3.88	3.88	10.4
	873	3.88	3.88	10.7
	973	3.88	3.88	11.2
V_2O_5/SiO_2	773	–	3.88	3.52

[a] Temperature range was 300–1123 K.

Fig. 5. FTIR spectra of CO adsorbed on Rh/SiO$_2$ and V–Rh/SiO$_2$ catalysts. The sample was exposed to CO at room temperature after H$_2$ reduction and evacuation at 573 K. The spectra were measured in vacuum at room temperature: (a) Rh/SiO$_2$ calcined at 773 K and (b) V–Rh/SiO$_2$ calcined at 973 K.

observed [46,47]: only the peak position of the bridge CO species was shifted. This may be reflected by the surface structure of V–Rh/SiO$_2$, although the reason is not clear at present. An important point is that main adsorbed species was changed to the linear CO. As shown in Table 3, in the case of Rh/SiO$_2$, the dispersion estimated from XRD was almost close to the CO/Rh ratio. However, in the case of V–Rh/SiO$_2$, the dispersion

estimated from XRD (0.37) was much higher than the corresponding CO/Rh (0.06). This disagreement can be explained by the covering of vanadium oxide species for Rh metal surface. This phenomenon has also been found on vanadia-modified Rh catalysts [18,25,48]. The ratio of the dispersion estimated from CO adsorption amount (0.06) to that from XRD (0.37) indicates that about 84% of the Rh surface is covered with vanadium oxide. Another interesting point is that over V–Rh/SiO$_2$ calcined at 973 K the amount of H$_2$ adsorption (H/Rh = 0.17) was much higher than that of CO adsorption (CO/Rh = 0.06). As shown in Table 3, on two Rh/SiO$_2$ catalysts, the adsorption amount of CO and H$_2$ was similar, which is consistent with the previous reports [18,25,48]. Furthermore, it has been known that the amount of CO adsorption was higher than that of H$_2$ adsorption over various modified Rh catalysts [49]. It can be interpreted as the additive component, destroying the surface ensemble for H$_2$ dissociation.

Fig. 6 shows the TEM images of V–Rh/SiO$_2$ catalyst calcined at 973 K after various treatments. The TEM image of V–Rh/SiO$_2$ after the calcination has already been reported [25], where large plate-type crystals assigned to RhVO$_4$ were observed clearly. After H$_2$ reduction, the presence of Rh metal particles was confirmed by XRD and TEM observation (Figs. 3(g) and 6(a)), and the particle size of Rh metal estimated from XRD was 3.0 nm (Table 3). This supports that the assembly of small particles in the TEM image are due to Rh metal particles, which also agrees with the previous reports [25,30]. The elemental analysis by energy dispersing X-ray analysis (EDX) suggested that the composition of the region of small particles assembly was
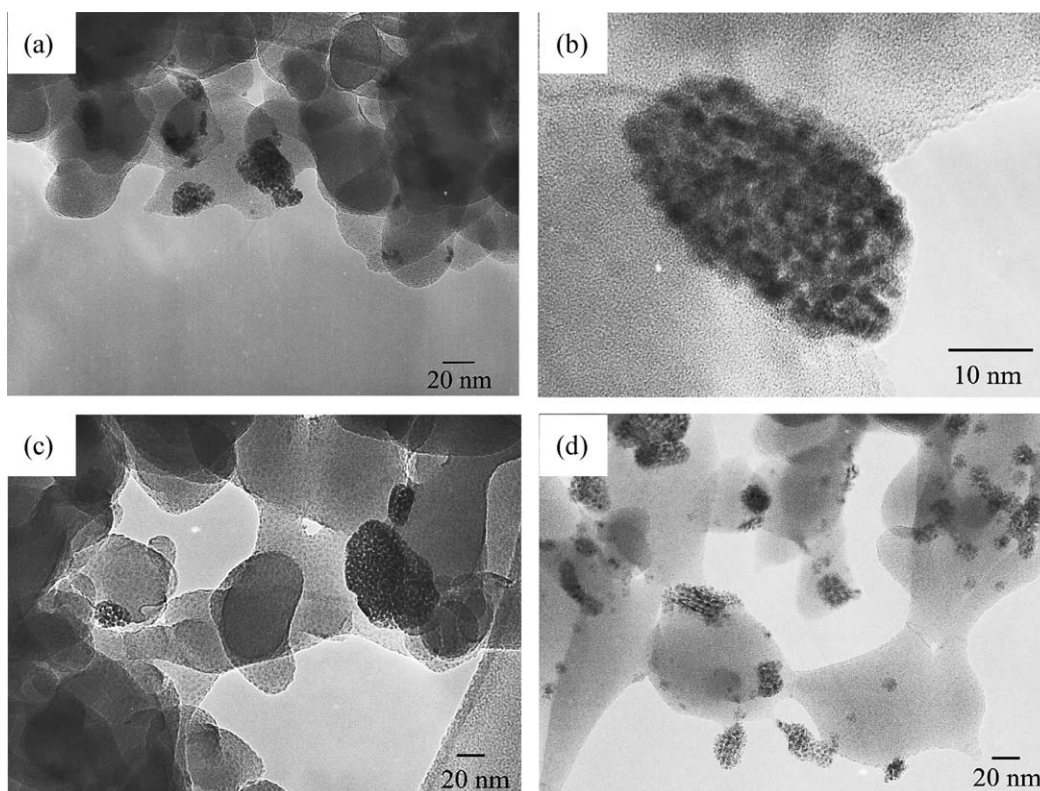

Fig. 6. TEM images of V–Rh/SiO$_2$ catalyst calcined at 973 K after various treatments: (a and b) after reduction at 573 K, (c) after hydroformylation of ethylene (reaction conditions are the same in Fig. 1) and (d) after CO hydrogenation (reaction conditions are the same in Table 7).

almost the same as that of the $RhVO_4$ crystal. This indicates that the interaction between Rh and vanadia is strong on the reduced catalyst, which can explain the fact that small metal particles do not aggregate in the assembly. It is also suggested that vanadia species are located between small Rh particles, and this can inhibit the aggregation of Rh metal particles. Fig. 6(b) shows the TEM image with higher magnification. It seems that metal particles with high contrast are covered with the lower contrast part, which can be assigned to vanadia species. In addition, the TEM observation of V–Rh/SiO$_2$ catalyst after ethylene hydroformylation showed no sintering of the Rh metal, and structural change was not observed after the reaction for 8 h (Fig. 6(c)).

On the basis of the amount of CO adsorption, the turnover frequency in hydroformylation was calculated, and the results are listed in Table 3. Since the CO adsorption and insertion is an important step in hydroformylation reaction, we used the data of CO adsorption in the TOF calculation. On two Rh/SiO$_2$ catalysts, the TOF of propanal formation was at a similar level. In contrast, the V–Rh/SiO$_2$ calcined at 973 K gave higher TOF of the formation of 1-propanol + propanal than that calcined at 773 K and those of two Rh/SiO$_2$ catalysts. This indicates that Rh modified with vanadia via $RhVO_4$ formation exhibited higher activity in ethylene hydroformylation.

3.3. Propanal hydrogenation under the presence of CO and model scheme of ethylene hydroformylation

As described above, the additive effect of vanadia to Rh/SiO$_2$ in hydroformylation reactions is to enhance the selectivity for alcohol formation as well as the TOF. In order to understand the mechanism of alcohol formation, we measured the activity of propanal hydrogenation in the presence of CO (Table 6). The pressure of CO and H$_2$ was adjusted to the hydroformylation conditions, and the pressure of propanal is determined from the result of ethylene hydroformylation. Two products, 1-propanol and 2-methyl-2-pentanal, were observed. The formation of 1-propanol is due to the hydrogenation of propanal, and the formation of 2-methyl-2-pentanal is due to the aldol condensation of propanal. Rh/SiO$_2$ showed very low activity in propanal hydrogenation. Mo-Rh/SiO$_2$ showed very high activity and selectivity to 1-propanol. In contrast, V–Rh/SiO$_2$ also showed high activity; however, the selectivity to 2-methyl-2-pentanal is much higher

than Mo-Rh/SiO$_2$. These results mean that propanal in the gas phase can be converted to 1-propanol and 2-methyl-2-pentanal over V–Rh/SiO$_2$. However, in the hydroformylation reaction over V–Rh/SiO$_2$, 2-methyl-2-pentanal was not observed at all. Therefore, it is thought that 1-propanol is formed without being via 1-propanal in the gas phase over V–Rh/SiO$_2$. This suggests that 1-propanol is formed directly from propanoyl species over V–Rh/SiO$_2$, which is a reaction intermediate of propanal formation, and it is thought that adsorbed acyl group is directly hydrogenated to alcohol via alkoxide species. Furthermore, the hydrogenation reaction can proceed in the presence of CO on V–Rh/SiO$_2$ and Mo-Rh/SiO$_2$, and this behavior is totally different from Rh/SiO$_2$. In the case of Rh/SiO$_2$, the hydrogenation reaction cannot proceed in the presence of CO since H$_2$ adsorption is inhibited by adsorbed CO species. These findings indicate that on the V–Rh/SiO$_2$ catalyst H$_2$ can be activated even in the presence of CO. As shown in Table 3, V–Rh/SiO$_2$ gave higher H/Rh than CO/Rh, and this suggests the presence of H$_2$ adsorption sites, which are not inhibited by adsorbed CO species.

In order to evaluate the ability of H$_2$ activation in the presence of CO, we measured the H$_2$–D$_2$ exchange reaction rate in the presence of CO. Fig. 7 shows Arrhenius plots of the reaction over Rh/SiO$_2$, V–Rh/SiO$_2$ and reduced V$_2$O$_5$/SiO$_2$. In the case of V$_2$O$_5$/SiO$_2$, on the basis of TPR results, the state of reduced V$_2$O$_5$/SiO$_2$ was adjusted to that of V–Rh/SiO$_2$, and the average state of vanadium was V^{3+} (V$_2$O$_3$). On the reduced V$_2$O$_5$/SiO$_2$, the exchange activity was too low to measure the rate accurately. On the other hand, Rh/SiO$_2$ exhibited the activity between V$_2$O$_5$/SiO$_2$ and V–Rh/SiO$_2$, and the activation energy was much higher than that on V–Rh/SiO$_2$. This is probably because H$_2$ is activated on the vacant Rh site under high CO coverage and the activation energy can include the energy of CO desorption [50].
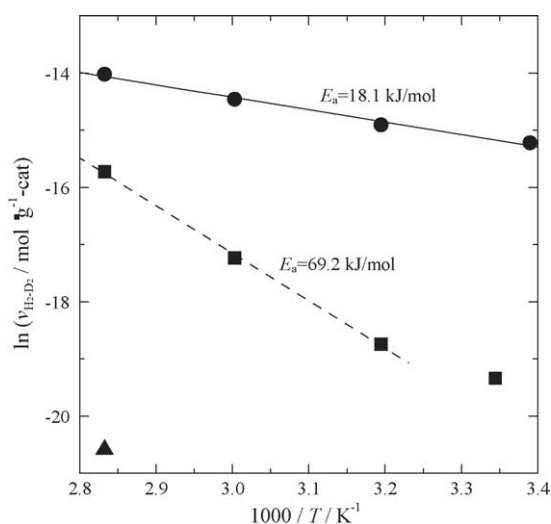

Fig. 7. Arrhenius plots of H$_2$–D$_2$ exchange reaction in the presence of CO: (■) Rh/SiO$_2$ calcined at 973 K, (●) V–Rh/SiO$_2$ calcined at 973 K and (▲) V$_2$O$_5$/SiO$_2$ calcined at 773 K. Reaction temperature range was from 299 to 353 K; $P_{H_2} = P_{D_2} = P_{CO} = 20.0$ kPa; Rh-based catalysts were reduced by H$_2$ at 573 K before reaction; V$_2$O$_5$/SiO$_2$ was reduced by H$_2$ at 1033 K before reaction.

Table 6
Results of $C_2H_5CHO + CO + H_2$ reaction at 388 K

Catalyst	Propanal-based conversion (%)	Selectivity (%)	
		1-Propanol	2-Methyl-2-pentanal
Rh/SiO$_2$[a]	1.7	0	100
V–Rh/SiO$_2$[b]	42.3	61	39
Mo-Rh/SiO$_2$[a]	70.1	99	1

Reaction conditions: catalyst weight 0.1 g, $P_{CO} = P_{H_2} = 33.8$ kPa, $P_{propanal} = 170$ Pa, total pressure = 0.1 MPa and total flow rate = 6 ml/min.
[a] Calcined at 773 K and reduced at 573 K.
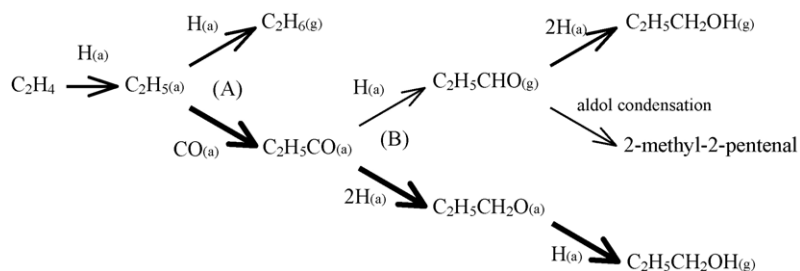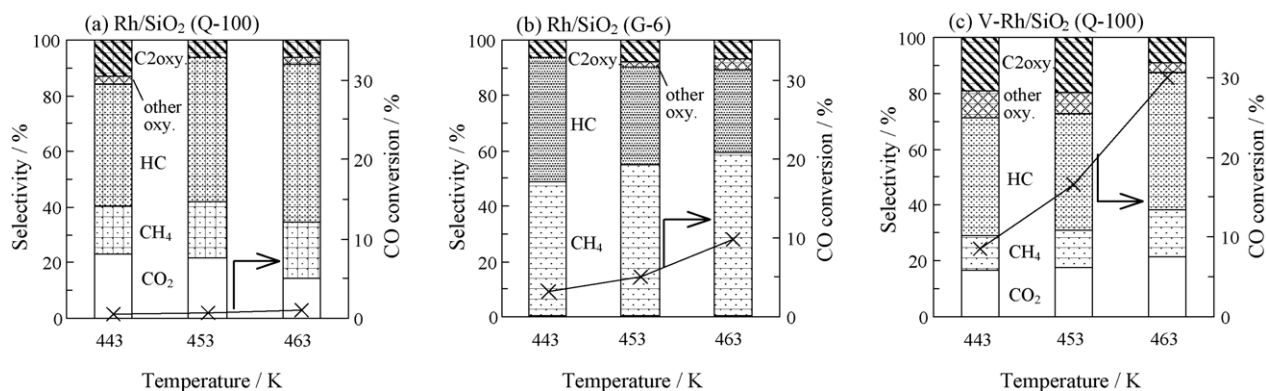[b] Calcined at 973 K and reduced at 573 K.

Fig. 8. Scheme of ethylene hydroformylation over V–Rh/SiO$_2$.

Fig. 9. Reaction temperature dependence of CO hydrogenation over Rh/SiO$_2$ (Q-100), Rh/SiO$_2$ (G-6) and V–Rh/SiO$_2$ (Q-100) catalysts: (a) Rh/SiO$_2$ (Q-100) calcined at 773 K, (b) Rh/SiO$_2$ (G-6) calcined at 773 K and (c) V–Rh/SiO$_2$ (Q-100) calcined at 973 K. Left axis: selectivity (%); right axis: CO conversion. Reaction conditions: catalyst weight = 0.5 g, P_{CO} = 33.8 kPa, P_{H_2} = 67.6 kPa, total flow rate = 1.5 ml/min, total pressure = 0.1 MPa and reduction temperature = 573 K.

The activation energy is similar to those of propanal and ethane formation in the hydroformylation of ethylene (Table 1). In contrast, V–Rh/SiO$_2$ exhibited high activity and lower activation energy. This result also supports the existence of H$_2$ activation sites over V–Rh/SiO$_2$, which are not inhibited by adsorbed CO species. In addition, since the active sites are not formed on reduced V$_2$O$_5$/SiO$_2$, the active sites can be located at the interface between Rh metal and vanadium oxide. The exchange rate

Table 7
CO conversion and selectivity in CO hydrogenation over Rh/SiO$_2$ and V–Rh/SiO$_2$ catalysts at 453 K

	Catalyst			
	Rh/SiO$_2$[a]		V–Rh/SiO$_2$[b]	
	Q-100 (1.5 h)[c]	G-6 (1.5 h)[c]	Q-100 (1.5 h)[c]	Q-100 (5.0 h)[c]
CO conversion (%)	0.6	5.0	16.6	14.2
Selectivity (%)				
Methanol	0.0	2.1	4.2	6.9
Ethanol	0.0	3.0	16.2	20.9
Acetaldehyde	0.3	2.9	2.0	2.5
Acetic acid	6.0	1.5	1.3	1.5
1-Propanol	0.0	0.0	3.5	3.1
CO$_2$	21.5	0.6	17.5	13.7
CH$_4$	20.3	54.6	13.6	13.9
HC				
C2	17.0	3.4	5.3	6.1
C3	25.2	13.2	13.5	12.3
C4	8.2	3.2	9.3	6.8
C5	1.6	7.7	5.1	4.1
C6	0.0	7.6	5.0	3.1
C7	0.0	0.0	3.5	5.2

Reaction conditions: catalyst weight = 0.5 g, P_{CO} = 33.8 kPa, P_{H_2} = 67.6 kPa, total flow rate = 1.5 ml/min, total pressure = 0.1 MPa and reduction temperature = 573 K.
[a] Calcined at 773 K.
[b] Calcined at 973 K.
[c] Support (reaction time).

was much higher than that of hydroformylation, and the activation energy was much lower. This indicates that H_2 adsorption can easily proceed, reaching equilibrium.

Fig. 8 shows a model scheme of ethylene hydroformylation and 1-propanol formation over V–Rh/SiO$_2$. The vanadia addition to Rh/SiO$_2$ influences the CO insertion (step A). It has been known that various additives are effective for the enhancement of hydroformylation selectivity [1,8–10]. This promotion can be explained by the interaction of oxygen atom of adsorbed CO on Rh with cations located near the Rh surface [9,51,52]. On the other hand, the addition of vanadia promoted 1-propaol formation. The path of 1-propanol formation is thought to be hydrogenation of propanoyl and propoxide species, or hydrogenation of propanal in the gas phase. From the result of propanal hydrogenation in the presence of CO, we assume that the main route is (B). This route is not opened over Rh/SiO$_2$. This is related to the ability of hydrogenation promoted by vanadia addition in hydroformylation reaction conditions. Particularly, the

interesting point is that the hydrogenation of propanoyl group is promoted more selectively than that of ethyl group judging from the TOF (Table 2). It is implied that the formation of propanoyl group and its hydrogenation can proceed at the same sites, which are located on Rh modified with vanadium oxide.

3.4. Effect of vanadia in CO hydrogenation

Fig. 9 shows reaction temperature dependence of CO hydrogenation over Rh/SiO$_2$ and V–Rh/SiO$_2$ catalysts. The details of product distribution are listed in Table 7. V–Rh/SiO$_2$ exhibited much higher CO conversion and selectivity to C2 oxygenates, especially ethanol, than two Rh/SiO$_2$ catalysts. As shown in Table 7, the CO conversion slightly decreased with time on stream. On the other hand, the TEM image (Fig. 6(d)) remained unchanged after H_2 reduction (Fig. 6(a)), and almost no change in the V/Rh ratio in that assembly was observed in EDX analysis
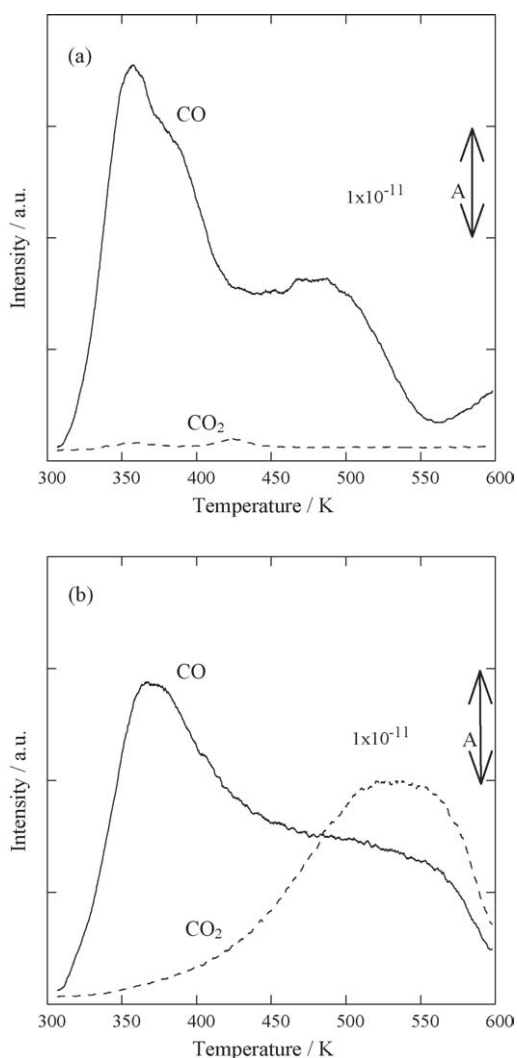

Fig. 10. Temperature-programmed desorption (TPD) profiles of CO adsorbed on Rh/SiO$_2$ and V–Rh/SiO$_2$ catalysts: (a) Rh/SiO$_2$ calcined at 773 K and (b) V–Rh/SiO$_2$ calcined at 973 K. Solid line: CO desorption; broken line: CO$_2$ desorption. The sample was exposed to CO at room temperature after H_2 reduction and evacuation at 573 K.
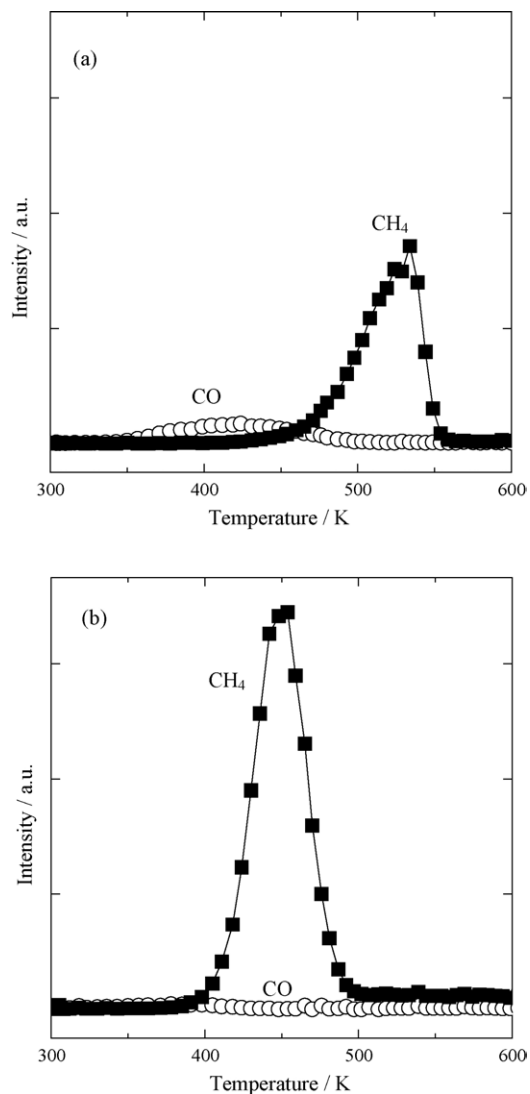

Fig. 11. Temperature-programmed surface reaction (TPSR) profiles of CO adsorbed on Rh/SiO$_2$ and V–Rh/SiO$_2$ in H_2 stream: (a) Rh/SiO$_2$ calcined at 773 K and (b) V–Rh/SiO$_2$ calcined at 973 K. Reduction temperature = 573 K and heating rate = 10 K/min. (○) CO and (■) CH$_4$.
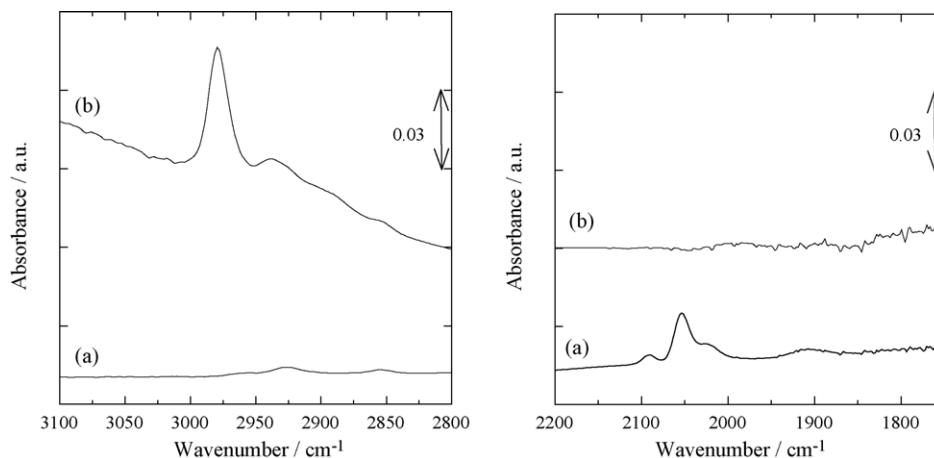
Fig. 12. FTIR spectra in C–H and CO stretching ranges of V–Rh/SiO$_2$ catalyst: (a) in vacuum after V–Rh/SiO$_2$ was exposed to CO at room temperature and (b) after (a) was exposed to H$_2$ at room temperature. Pretreatment: calcination temperature = 973 K and reduction temperature = 573 K.

(0.58–0.55). From this result, it is suggested that the decrease in CO conversion cannot be due to structural change of the catalyst, but due to the accumulation of carbon or higher hydrocarbon [53]. The vanadia modification clearly enhanced the CO conversion and the selectivity to C2 oxygenates formation. Although the reaction temperature for CO hydrogenation was higher than that for hydroformylation, the effect of vanadia addition on the selectivity for alcohol formation can be explained as described in the section of hydroformylation.

Fig. 10 shows CO-TPD on Rh/SiO$_2$ and V–Rh/SiO$_2$. In the case of Rh/SiO$_2$, the CO desorption was observed at 360 and 475 K, and almost no CO$_2$ was observed. In contrast, in the TPD profile of V–Rh/SiO$_2$, CO$_2$ desorption was observed clearly at higher temperature range. This indicates that CO disproportionation reaction (2CO → C + CO$_2$) over V–Rh/SiO$_2$ can proceed much more easily compared to Rh/SiO$_2$, and this means that CO dissociation is promoted by vanadia addition.

Fig. 11 shows TPSR profiles of adsorbed CO in the flow of H$_2$. In the case of Rh/SiO$_2$, small amount of CO was desorbed above 350 K, and adsorbed CO was mainly hydrogenated to CH$_4$ above 450 K. In contrast, CO adsorbed on V–Rh/SiO$_2$ was hydrogenated at lower temperature (380 K) than that over Rh/SiO$_2$. In both cases, the main product is methane, and the simple desorption of CO, which was observed in the TPD profiles, is inhibited under the H$_2$ flow. To elucidate this behavior, we measured FTIR spectra of CO adsorption in H$_2$ flow (Fig. 12). Before adsorbed CO was exposed to H$_2$, twin, linear and bridge CO species were observed (Fig. 12(a)). When the sample was exposed to H$_2$ at room temperature, CO adsorption peaks disappeared, and the peaks at 2980 and 2938 cm^{-1} appeared (Fig. 12(b)). These species can be assigned to methylidyne and methyl species, respectively, on the basis of the previous reports [54,55]. This result indicates that CO dissociation is drastically promoted by the presence of H$_2$. In addition, the TPSR result shows that this effect was much more significant on V–Rh/SiO$_2$ than on Rh/SiO$_2$. It is thought that the interface between Rh metal and vanadium oxide can play a very important role in the CO dissociation step promoted by H$_2$, because the oxygen atom of CO

adsorbed on Rh can interact with vanadium oxide, and H$_2$ activation is not inhibited by adsorbed CO.

4. Conclusions

1. The effect of addition of vanadia to Rh/SiO$_2$ was highly dependent on the calcination temperature, and this was due to the formation of RhVO$_4$ mixed oxide phase.
2. In the hydroformylation of ethylene, the addition of vanadia drastically promoted the formation of 1-propanol. The promoting effect was more significant on the catalyst calcined at high temperature. Rh and V species on the reduced catalyst became more intimate when formed by the decomposition of RhVO$_4$ in H$_2$.
3. In the hydroformylation of ethylene over V–Rh/SiO$_2$, the addition of vanadia promoted CO insertion to the ethyl group and 1-propanol formation. The promotion of CO insertion can be due to the interaction between CO adsorbed on Rh and vanadia, which is expected from the CO$_2$ formation observed in the CO-TPD result.
4. The route of 1-propanol formation over V–Rh/SiO$_2$ catalyst is hydrogenation of propanoyl group and propoxide group as suggested by the result of propanal hydrogenation in the presence of CO.
5. The hydrogenation promoted by vanadia addition is related to adsorption of hydrogen, which is not inhibited by CO adsorption. This is supported by adsorption measurements (H/Rh > CO/Rh on V–Rh/SiO$_2$) and H$_2$–D$_2$ exchange reaction in the presence of CO.
6. In CO hydrogenation, the addition of vanadia to Rh/SiO$_2$ drastically enhanced CO conversion and selectivity for ethanol formation. Ethanol formation can be related to the high selectivity for 1-propanol formation in ethylene hydroformylation.
7. CO-TPD suggested that vanadia addition promoted CO dissociation, and furthermore, the TPSR result indicates that the effect became more remarkable in the presence of hydrogen.

References

[1] M. Ichikawa, Polyhedron 7 (1988) 2351.

[2] S.S.C. Chuang, S.I. Pien, J. Mol. Catal. 55 (1989) 12.

[3] S.A. Hedrick, S.S.C. Chuang, A. Pant, A.G. Dastidar, Catal. Today 55 (2000) 247.

[4] B.T. Li, X. Li, K. Asami, K. Fujimoto, Chem. Lett. 32 (2003) 378.

[5] B.T. Li, X. Li, K. Asami, K. Fujimoto, Energy Fuels 17 (2003) 810.

[6] E. Mantovani, N. Palladino, A. Zanobi, J. Mol. Catal. 3 (1978) 285.

[7] G. Alagona, C. Ghio, R. Lazzaroni, R. Settambolo, Organometallics 20 (2001) 5394.

[8] W.M.H. Sachtler, M. Ichikawa, J. Phys. Chem. 90 (1986) 4752.

[9] A. Fukuoka, M. Ichikawa, J.A. Hriljac, D.F. Shriver, Inorg. Chem. 26 (1987) 3643.

[10] A. Fukuoka, L.F. Rao, N. Kosugi, H. Kuroda, M. Ichikawa, Appl. Catal. 50 (1989) 295.

[11] A. Trunschke, H.-C. Böttcher, A. Fukuoka, M. Ichikawa, H. Miessner, Catal. Lett. 8 (1991) 221.

[12] T. Hanaoka, H. Arakawa, T. Matsuzaki, Y. Sugi, K. Kanno, Y. Abe, Catal. Today 58 (2000) 271.

[13] L. Huang, A. Liu, Y. Xu, J. Mol. Catal. 124 (1997) 57.

[14] Y. Izumi, Y. Iwasawa, J. Phys. Chem. 96 (1992) 10942.

[15] A. Fusi, R. Psaro, C. Dossi, L. Garlaschelli, F. Cozzi, J. Mol. Catal. A 107 (1996) 255.

[16] H. Arakawa, K. Takeuchi, T. Matsuzaki, Y. Sugi, Chem. Lett. (1984) 1607.

[17] G. van der Lee, B. Schuller, H. Post, T.L.F. Favre, V. Ponec, J. Catal. 98 (1986) 522.

[18] B.J. Kip, P.A.T. Smeets, J. van Grondelle, R. Prins, Appl. Catal. 33 (1987) 181.

[19] J. Kowalski, G. van der Lee, V. Ponec, Appl. Catal. 19 (1985) 423.

[20] A.B. Boffa, A.T. Bell, G.A. Somorjai, J. Catal. 139 (1993) 602.

[21] A.B. Boffa, C. Lin, A.T. Bell, G.A. Somorjai, Catal. Lett. 27 (1994) 243.

[22] S. Ishiguro, S. Ito, K. Kunimori, Catal. Today 45 (1998) 197.

[23] S. Ito, S. Ishiguro, K. Kunimori, Catal. Today 44 (1998) 145.

[24] S. Ito, T. Fujimori, K. Nagashima, K. Yuzaki, K. Kunimori, Catal. Today 57 (2000) 247.

[25] S. Ito, C. Chibana, K. Nagashima, S. Kameoka, K. Tomishige, K. Kunimori, Appl. Catal. A 236 (2002) 113.

[26] J.Y. Shen, T. Matsuzaki, T. Hanaoka, K. Takeuchi, Y. Sugi, Catal. Lett. 28 (1994) 329.

[27] C. Mazzacchia, P. Gronchi, A. Kaddouri, E. Tempesti, L. Zanderighi, A. Kiennemann, J. Mol. Catal. A 165 (2001) 219.

[28] J. Schoiswohl, M. Sock, S. Eck, S. Surnev, M.G. Ramsey, F.P. Netzer, Phys. Rev. B 69 (2004) 155403.

[29] T. Beutel, V. Siborov, B. Tesche, H. Knözinger, J. Catal. 167 (1997) 379.

[30] B. Tesche, T. Beutel, H. Knözinger, J. Catal. 149 (1994) 100.

[31] Z. Hu, T. Wakasugi, A. Maeda, K. Kunimori, T. Uchijima, J. Catal. 127 (1991) 276.

[32] Z. Hu, H. Nakamura, K. Kunimori, H. Asano, T. Uchijima, J. Catal. 112 (1988) 478.

[33] B.D. Cullity, Elements of X-Ray Diffraction, 1978.

[34] K. Kunimori, T. Uchijima, M. Yamada, H. Matsumoto, T. Hattori, Y. Murakami, Appl. Catal. 4 (1982) 67.

[35] Z. Hu, H. Nakamura, K. Kunimori, Y. Yokoyama, H. Asano, M. Soma, T. Uchijima, J. Catal. 119 (1989) 33.

[36] N. Takahashi, S. Hasegawa, N. Hanada, M. Kobayashi, Chem. Lett. (1983) 945.

[37] M.W. Balakos, S.S.C. Chuang, J. Catal. 151 (1995) 266.

[38] N. Takahashi, Y. Sato, T. Uchiumi, K. Ogawa, Bull. Chem. Soc. Jpn. 66 (1993) 1273.

[39] L. Huang, Y. Xu, W. Guo, A. Lin, D. Li, X. Guo, Catal. Lett. 32 (1995) 61.

[40] H. Arakawa, N. Takahashi, T. Hanaoka, K. Takeuchi, T. Matsuzaki, Y. Sugi, Chem. Lett. (1988) 1917.

[41] X-Ray Powder Diffraction Data File, ICDD 00-041-0134.

[42] K. Kunimori, T. Wakasugi, F. Yamakawa, H. Oyanagi, J. Nakamura, T. Uchijima, Catal. Lett. 9 (1991) 331.

[43] X-Ray Powder Diffraction Data File, ICDD 00-030-0848.

[44] X-Ray Powder Diffraction Data File, ICDD 00-016-0311.

[45] X-Ray Powder Diffraction Data File, ICDD 00-001-1053.

[46] S.D. Worley, G.A. Mattson, R. Caudlll, J. Phys. Chem. 87 (1983) 1671.

[47] C.A. Rice, S.D. Worley, C.W. Curtis, J.A. Guin, A.R. Tarrer, J. Chem. Phys. 74 (1981) 6487.

[48] B.J. Kip, P.A.T. Smeets, J.H.M.C. van Wolput, H.W. Zandbergen, J. van Grongelle, Appl. Catal. 33 (1987) 157.

[49] K. Tomishige, K. Asakura, Y. Iwasawa, J. Catal. 149 (1994) 70.

[50] B. Klötzer, W. Unterberger, K. Hayek, Surf. Sci. 532 (2003) 142.

[51] T. Fukushima, H. Arakawa, M. Ichikawa, J. Chem. Soc. Chem. Commun. (1985) 729.

[52] M. Ichikawa, A.J. Lang, D.F. Shriver, W.M.H. Sachtler, J. Am. Chem. Soc. 107 (1985) 7216.

[53] S. Ito, C. Chibana, K. Nagashima, S. Kameoka, K. Tomishige, K. Kunimori, J. Jpn. Petrol. Inst. 45 (2002) 251.

[54] J. Kiss, A. Kis, F. Solymosi, Surf. Sci. 454–456 (2000) 273.

[55] J. Manna, R.F. Dallinger, V.M. Miskowski, M.D. Hopkins, J. Phys. Chem. 104 (2000) 10928.